A numerical study on the effects of operational parameters and membrane characteristics on the performance of vacuum membrane distillation (VMD)

Muhammad Suleman[a], Muhammad Asif[a,b], Syed Asad Jamal[a], Pengyu Dong[b,*], Xinguo Xi[c,*]

[a]*Faculty of Mechanical Engineering, GIK Institute of Engineering Sciences and Technology, Topi 23460, Pakistan,
Tel. +92-343-9194005; email: gme1833@giki.edu.pk (M. Suleman), Tel. +92-303-5522706; email: masif@giki.edu.pk (M. Asif),
Tel. +92-334-3311574; email: gme1839@giki.edu.pk (S.A. Jamal)*
[b]*Key Laboratory for Advanced Technology in Environmental Protection of Jiangsu Province, Yancheng Institute of Technology,
Yancheng 224051, PR China, Tel. +86-515-88298923; email: dongpy11@gmail.com (P. Dong)*
[c]*School of Chemistry & Chemical Engineering, Yancheng Institute of Technology, Yancheng 224051, PR China,
Tel. +86-515-88298186; email: xxg@ycit.cn (X. Xi)*

ABSTRACT

Recently, the seawater desalination process has gained widespread attention due to lack of drinking water. Among several membrane distillation methods for desalination, vacuum membrane distillation (VMD) is one of the emerging technologies that has mostly focused. In this study, an integrated heat and mass transfer model for the VMD process is established and the simulation results are validated with experimental data available in the literature. The numerical model is solved using in-house coding in Mathcad. The effect of some influential process parameters like feed circulation velocity, feed temperature, salinity, and heat transfer coefficient (HTC) on VMD flux is investigated. Moreover, the influence of some membrane characteristics like membrane porosity, membrane pore size and membrane thickness on permeate flux is also considered. Furthermore, the effect of some operating parameters on temperature polarization is also presented in this paper. Results of the numerical model indicated that the VMD flux enhanced with an increase in velocity, feed temperature, membrane porosity, membrane pore size, and HTC, whereas permeate flux declined with an increase in salt concentration, vacuum pressure, and membrane thickness. The maximum increase in permeate flux was 21.62 kg/m²h by increasing feed temperature from 35°C to 65°C at a constant feed velocity of 1.0 m/s. Additionally, it was confirmed that an optimum value of the membrane parameter is preferable for a substantial improvement in overall VMD performance.

Keywords: Heat transfer; Mass transfer; Membrane distillation; Permeate flux; Temperature polarization; Vacuum membrane distillation; VMD

1. Introduction

The earth is composed of 70% water, out of which 97% is in the oceans and is not drinkable because of its salty nature [1,2]. The remaining freshwater is not directly accessible because it is present in the deep aquifers. As a result, the shortage of fresh water has become a global issue and society has arrived at the problem of shortage of drinkable water. However, this problem may be addressed by the desalination of seawater to make it drinkable. Various techniques are available to desalinate seawater such as multi-stage flash distillation (MSF), multi-effect distillation (MED) and reverse osmosis (RO). All of these techniques require higher operating and maintenance costs, and they cannot be operated by

* Corresponding authors.

means of a low-grade energy source such as solar energy [3]. An alternative to existing methods of seawater desalination is membrane distillation (MD) which has emerged as an alternative and attractive technique to common processes such as MED, MSF and RO [4].

MD process revealed many appealing features, particularly when integrated with a low-grade heat source such as low operating pressure and temperature, simple membrane construction, little consumption of energy when waste heat is available, theoretically 100% salt rejection, high potential to use a low-grade energy source and no extensive pretreatment [4–8].

MD exists in the form of four different modules based on the process arrangements: direct contact membrane distillation (DCMD), vacuum membrane distillation (VMD), air gap membrane distillation (AGMD) and sweeping gas membrane distillation (SGMD) [9–11]. The main difference in these configurations lies in the type of condensing design (cold side) and are categorized based on the method by which pressure difference is generated across the membrane. In DCMD [12], the cold stream at the permeate side is in direct contact with the membrane surface. This cold stream cannot cross the membrane pores and is a condensing medium for the vapors that are transported from the membrane feed side. In AGMD [13], the feed solution and membrane are only in direct contact and the transported vapors are condensed on the cold surface. The existence of air gap between the condensing surface and the membrane decreases the heat loss, and as a result, improved thermal efficiency compared to DCMD. However, a major disadvantage of AGMD is that it offers resistance to the permeate flux and as a result imposes a high mass transfer resistance compared to other MD modules. In SGMD, an inert gas is used that sweeps the vapors. In this configuration, the condensation of the vapor takes place outside the MD module [14]. In VMD, vacuum pressure is created at the membrane permeate side and because of this vacuum pressure, a partial vapor pressure difference is created across the membrane. This pressure difference is responsible for the transport of vapors through the membrane. A comparison between MD configurations shows that the VMD process involves low mass transfer resistance and can produce permeate flux at a low operating temperature [15,16]. In addition to seawater desalination, VMD is also being used for fermentation [17,18], juice and coffee concentration in the food industry [19–26], removal of volatile organic compounds from aqueous solution [27–36], mineral recovery [37], and for regeneration of liquid desiccant air conditioning system [38,39].

To accurately predict the permeate flux and also the behavior of heat and mass transfer in a VMD configuration, a detailed integrated heat and mass transfer model (HMTM) is essentially required. By exploring the previously reported prominent articles on VMD, few studies can be found related to the effects of operational parameters on permeate flux and temperature polarization (TP) phenomenon in VMD [40,41], and also a very limited work related to the effects of membrane characteristics on the performance of VMD can be found in the literature [42]. Likewise, the only membrane characterization parameter considered in the past to study its effect on the TP is the membrane thickness [42]. However, no attempt can be found in the open literature that considered the effects of other membrane characterization parameters (i.e. mean pore size, membrane porosity, etc.) on the TP phenomenon in VMD. Accordingly, the purpose of this study was to fill the required gap. TP is one of the main drawbacks associated with VMD that notably influences the permeate flux and largely depends on the process parameters and membrane characteristics. Thus, an attempt was made to study the effects of different membrane characteristics and process parameters on the permeate flux and TP to get enhanced permeate flux and improved VMD performance. In this study, an integrated HMTM for the VMD process has been established. The model is solved using in-house coding in Mathcad. The simulation results are validated with the experimental data [43] of the previously published literature.

2. Theory

2.1. Mass transfer model

The microporous membrane is responsible for the vapors transport in MD by allowing the diffusive and conductive flow of vapors through the membrane pores. The difference between the pressure at the feed side and the vacuum pressure is responsible for mass transfer in VMD. The membrane structure itself is the main barrier to vapors transport. Moreover, the air present within the membrane pores also imposes a resistance for the mas transfer. The mass transfer in VMD can be explained by either Poiseuille model or Knudsen diffusion model, the prior being dominant when the mean free molecular path of the gaseous water molecules is smaller than the membrane pore size [44], whereas Knudsen diffusion is dominant in case of smaller pore size compared to the mean free molecular path [28,45]. The following equation is used to calculate mass flux in case of Knudsen model:

$$J_k = 1.064 \frac{r\varepsilon}{\tau\delta} \left(\frac{M}{RT_{avg}} \right)^{0.5} \left(P_i - P_v \right) \tag{1}$$

where P_v and P_i are water vapor pressure at vacuum side and feed side at membrane interface respectively; r, δ, τ and ε are the pore size, membrane thickness, tortuosity, and membrane porosity respectively; and T_{avg}, R, and M are average absolute temperature in membrane pores, universal gas constant and molecular weight of water, respectively.

On the other hand, for Poiseuille's flow regime the equation used is:

$$J_p = 0.125 \frac{r^2\varepsilon}{\tau\delta} \left(\frac{MP_{avg}}{\eta RT_{avg}} \right) \left(P_i - P_v \right) \tag{2}$$

where P_{avg} and η are average vapor pressure and viscosity of water vapor respectively.

Dimensionless number called Knudsen number is used to specify the flow type, which is described as follows:

$$Kn = \frac{\lambda}{L} \tag{3}$$

In Eq. (3) λ is the mean free molecular path and L is a physical scale characteristic length [46]. In this study, the characteristic length would be the membrane pore size. In most VMD arrangements, the mean free molecular path is extremely larger as compared to the pores size of the membrane. For that reason, the Knudsen model usually controls the mass transfer across the membrane.

2.2. Heat transfer model

Depends on the process arrangement, three types of heat transfers are involved in the VMD process; (1) the heat transfer through the membrane by means of conduction. (2) The heat transfer by means of convection from the feed side boundary layer adjacent to the membrane interface. (3) The latent heat transfer associated with permeate flux.

The convection heat transfer from the feed side boundary layer can be defined as:

$$Q_f = h_f\left(\pi d_0 N_f\right)\left(T_b - T_i\right) \tag{4}$$

where h_f is the convective heat transfer coefficient (HTC). Groehn's correlation can be used to find h_f [47]:

$$N_u = \frac{h_f d_h}{K_f} = 0.206\left(\mathrm{Re}\cos\theta\right)^{0.63}\mathrm{Pr}^{0.36} \tag{5}$$

where d_h is the hydraulic diameter of the shell, K_f is the thermal conductivity and θ is the yaw angle which varies from 0° to 90°. In our case, the yaw angle is 87° for the MD020CP2N membrane module [7].

For calculating Reynold's number, the following relation can be used:

$$\mathrm{Re} = \frac{d_h \rho v}{\mu} \tag{6}$$

where ρ, v, and μ are the density, velocity, and viscosity of the feed solution, respectively.

Also, the Prandtl number (Pr) can be calculated by using the following relation:

$$\mathrm{Pr} = \frac{C_p \mu}{K} \tag{7}$$

The hydraulic diameter of the shell can be computed by using the following relation:

$$d_h = \frac{d_0\left(1-\varnothing\right)}{\varnothing} \tag{8}$$

where $\varnothing$ is the module property known as module packing density.

$$\varnothing = N_f\left(\frac{d_0}{d_s}\right)^2 \tag{9}$$

where d_s is the shell inner diameter.

It must be noted that in the steady-state conditions, the heat transfer in the feed side and the heat transfer through the membrane are equal [43,44,48].

$$Q_f = Q_m \tag{10}$$

2.3. Integration of heat and mass transfer

In the VMD process, the heat and mass transfer rates are interconnected. A change in one of them induces a change in the other. According to Alsaadi et al. [49], the two rates are related by the following equation:

$$Q = h_f\left(T_b - T_i\right) = Jg_v = C_m\left(P_i - P_v\right)g_v \tag{11}$$

where g_v and C_m are enthalpy of saturated vapor and mass permeability coefficient of the membrane, respectively. To calculate g_v, we used the following equation [50]:

$$\begin{aligned} g_v = {} & 2501.689845 + 1.806916015T + 5.087717\times10^{-4}T^2 - \\ & 1.1221\times10^{-5}T^3 \end{aligned} \tag{12}$$

where T is valid in the range 0.01–200°C.

2.4. Temperature polarization

A primary reason for flux declination during the MD operation is the TP near the membrane interface. As can be seen in Fig. 1, the feed bulk temperature T_b drops to T_i at the membrane interface on the feed side. Some water evaporates and is transported through the membrane pores to the permeate side. At the same time, heat is transferred through the membrane. The force which is responsible for vapors transport is, therefore, the pressure difference between the feed side at temperature (T_i) and the vacuum pressure at the lumen side, which is less than the difference in pressure between the feed side at bulk temperature (T_b) and the vacuum pressure. So the driving force for vapors transport should be less in this case. This phenomenon is called TP [51–54].

The TP effect can be expressed mathematically by a factor known as temperature polarization coefficient (TPC) which can be defined as the ratio of the temperature difference between the feed side membrane interface temperature and the permeate side temperature to the difference between the bulk temperatures across both the membrane sides;

$$\mathrm{TPC} = \frac{T_i - T_v}{T_b - T_v} \tag{13}$$

According to Eq. (14), lower the value of TPC, more extensive is the TP. Consequently, the difference between interface temperature T_i and feed bulk temperature T_b turns out to be much greater and the resistance to mass transfer increases. On the other hand, as TPC value approaches to unity, the TP effect turns out to be trivial, the temperature gradient at the feed side becomes smaller and the system will be only mass transfer limited.
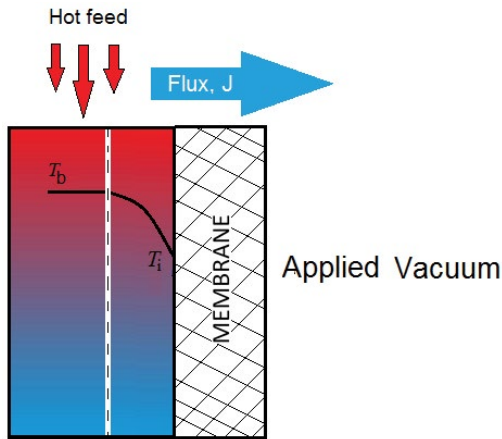
Fig. 1. Temperature polarization in VMD.

3. Methodology

3.1. Input parameters

To get more flux and also to enhance the VMD performance, a simultaneous HMTM for the VMD process is established and the results are validated with the experimental data of the previously published literature. The numerical model has been solved using in-house coding in Mathcad. The calculations were carried out for a feed circulation velocity of 0.2 m/s, feed temperature of 50°C and for a vacuum pressure of 2,000 Pa. The calculations were carried out for a polypropylene (PP) hollow fiber membrane with a porosity of 0.7 and a thickness of 400 μm. To study the effects of operating parameters on permeate flux and TP, a numerical iterative method as discussed in section 3.3 was adopted.

3.2. Membrane properties

Properties of the MD020CP2N hollow fiber membrane module was used in the numerical model. A schematic of the hollow fiber membrane module is shown in Fig. 2. The hollow fiber membrane module has three layers; shell side through which feed solution flows, the membrane layer and the permeate side which should be kept under vacuum. The MD020CP2N is a commercial shell and tube type hollow fiber membrane module in which the feed solution flows in the shell side whereas the lumen side is kept under vacuum. It contains a set of PP porous hollow fibers which are hydrophobic. The properties of MD020CP2N membrane module specified by the manufacturer are as follows:

Length of fibres: 0.47 m; number of fibres: 40; inner diameter of the shell: 0.025 m; inner diameter of fibres: 1.8 mm; outer diameter of fibres: 2.6 mm; thickness of membrane: 0.4 mm; membrane mean pore size: 0.2 μm; effective area: 0.15 m²; porosity of the membrane module: 70%.

3.3. Solution procedure

The thermophysical properties of NaCl solution and water were used from the reference [55]. A flow chart of the solution procedure is shown in Fig. 3. A numerical iterative
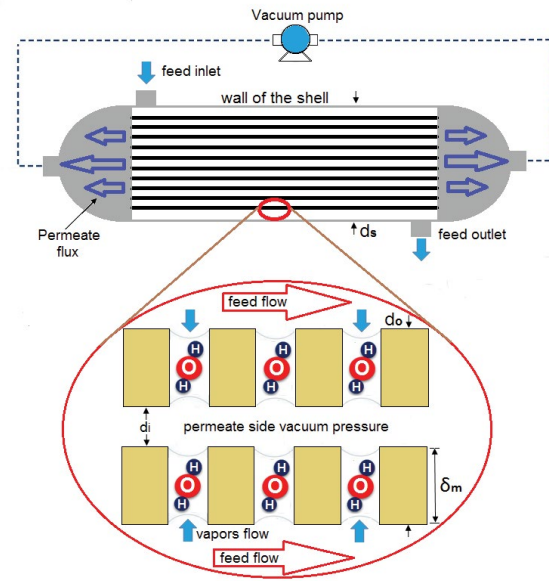

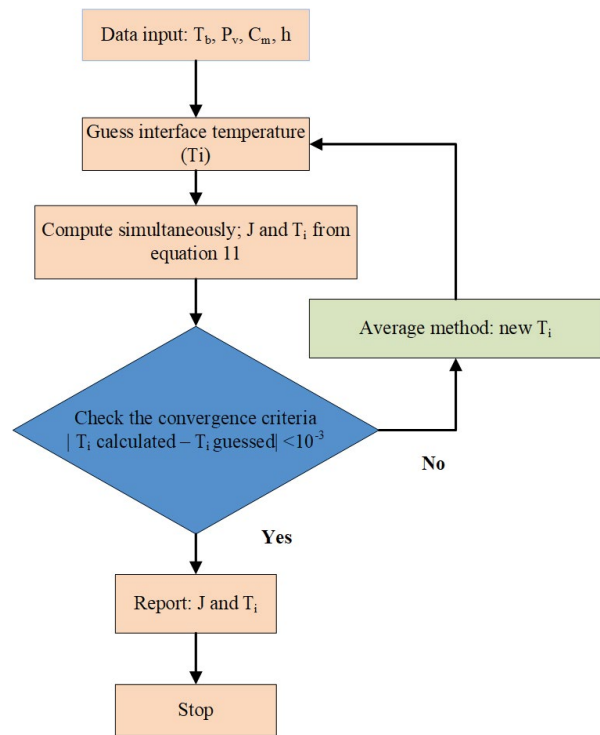Fig. 2. Schematic representation of a hollow fiber VMD module.

Fig. 3. VMD model iteration.

method is used to solve for the value of permeate flux and the membrane interface temperature using Mathcad's in-house coding. HTC is found from Groehn's correlation [47]. g_v is calculated using Eq. (12) whereas P_v is calculated from Antoine's equation:

$$P_v = \exp\left(23.1964 - \frac{3816.44}{-46.13 + T}\right) \tag{14}$$

The membrane interface temperature and the permeate flux should be estimated on a trial basis. The solution was converged when the calculated interface temperature and the guessed temperature were satisfied within an absolute error of 10^{-3}.

4. Validation of numerical model

It is of interest to relate the numerical findings with the experimental results. The numerical model was compared with the experimental results of Mengual et al. [43]. The model was validated by comparing the experimental and numerically determined to permeate flux over a range of feed temperatures from 35°C to 65°C and was also compared over a range of feed velocities from 0.2 to 1.0 m/s as shown in Figs. 4a and b, respectively. The lines and symbols depict the numerical and experimental results respectively. As shown in Figs. 4a and b, the numerical results show a good agreement with the experimental data, with an average deviation of less than 5% between the simulated and experimental flux.
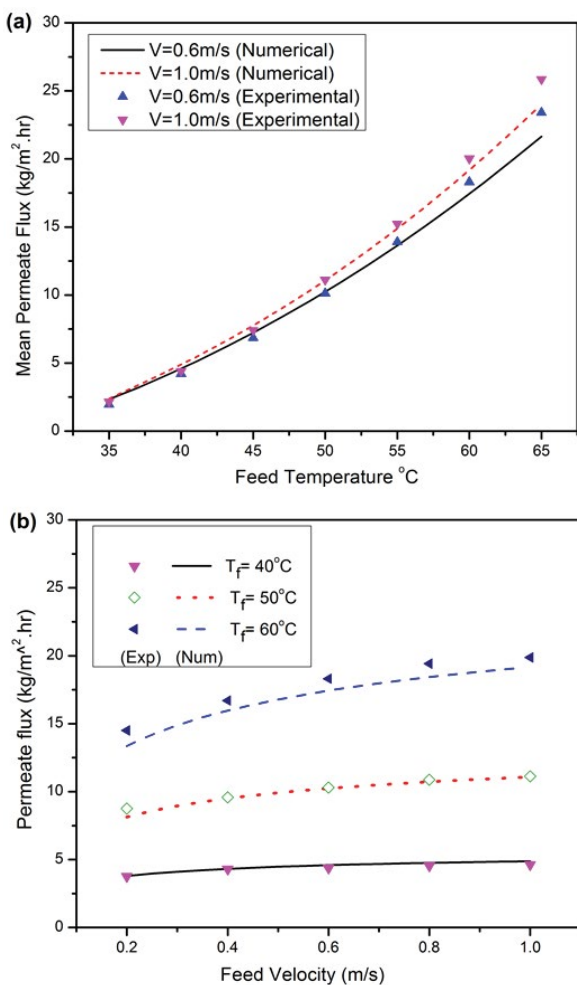

Fig. 4. Comparison of numerical and experimental permeate flux (a) feed temperature at feed velocity (*V*) of 0.6 and 1.0 m/s, (b) feed velocity at feed temperature (T_f) of 40°C, 50°C, and 60°C. Lines: numerical data and symbols: experimental data.

5. Numerical results and discussion

5.1. Effect of operating parameters on permeate flux

5.1.1. Feed temperature

The influence of feed temperature on VMD flux is shown in Fig. 5 at various feed circulation velocities. The temperature was varied from 35°C to 65°C, for each one of the following feed velocities: 0.2, 0.4, 0.6, 0.8 and 1.0 m/s. While increasing feed temperature, an increase in permeate flux occurs because of the exponential relationship between vapor pressure and temperature as given by Antoine's equation. Therefore, a rise in feed temperature will result in increased vapor pressure of the feed solution that will, in turn, increase the permeate flux.

As depicted in the figure, at low feed temperature, the impact of velocity variation is low, whereas, at a high feed temperature of 65°C, the flux is enhanced from 16.3 to 24 kg/m²h by increasing velocity from 0.2 to 1 m/s. Likewise, when the feed velocity was 0.2, 0.4, 0.6, 0.8, and 1.0 m/s and the feed temperature is varied from 35°C to 65°C, the flux increased from 1.94 to 16.3 kg/m²h, from 2.21 to 19.69 kg/m²h, from 2.34 to 21.64 kg/m²h, from 2.37 to 22.98 kg/m²h and from 2.38 to 24 kg/m²h, respectively. The maximum increase in permeate flux is 21.62 kg/m²h at a feed circulation velocity of 1.0 m/s. Hence, initially at lower feed temperature, the effect of increase in velocity is insignificant however the effect becomes dominant by increasing the feed temperature.

5.1.2. Feed velocity

Fig. 6 presents the numerical values of permeate flux against feed velocity using the feed temperature as variable. The velocity was varied from 0.2–1.0 m/s, for each one of the following feed temperatures: 40°C, 50°C, and 60°C. An increase in feed circulation velocity led to an increase in the HTC and as a result, the membrane interface temperature became closer to the feed bulk temperature. This will cause a higher temperature difference across the membrane and subsequently a higher flux.
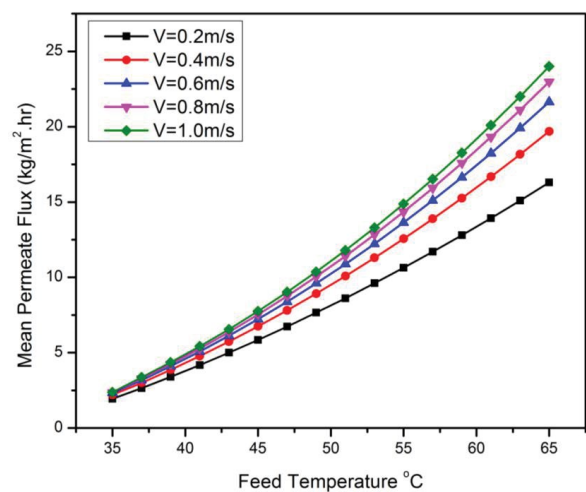

Fig. 5. Effect of feed temperature on permeate flux for water inlet velocity (*V*) of 0.2, 0.4, 0.6, 0.8, and 1.0 m/s.
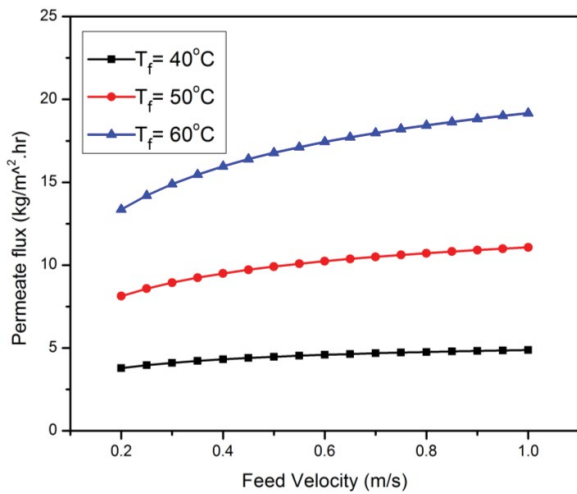
Fig. 6. Effect of feed circulation velocity on VMD flux for inlet feed temperature (T_f) of 40°C, 50°C, and 60°C.

Fig. 7. Effect of vacuum pressure on MD flux for inlet feed temperature (T_f) of 50°C, 60°C, and 70°C.

While feed temperature is 40°C, 50°C, and 60°C and the feed circulation velocity is varied from 0.2–1.0 m/s, permeate flux increased from 3.79 to 4.88 kg/m²h, from 8.13 to 11.07 kg/m²h and from 13.36 to 19.17 kg/m²h respectively. The maximum increase in permeate flux is 5.81 kg/m²h at a temperature of 60°C. Moreover, the impact of feed velocity on permeate flux is trivial at low values of feed temperature. However, the effect becomes dominant with the increase in feed temperature.

5.1.3. Vacuum pressure

In the VMD performance, vacuum pressure at the permeate side plays a significant role. The effect of vacuum pressure on the permeate flux is studied for three different feed temperatures (i.e., 50°C, 60°C, and 70°C) as shown in Fig. 7, while keeping the feed flow rate constant at 0.2 m/s. As it is clear, while vacuum pressure increased, MD flux declined for all three feed temperatures. This is because of the decrease in the driving force required for MD mass transport, since the difference in vapor pressure at feed side temperature and the vacuum pressure is responsible for mass transfer in MD. Therefore, MD flux increased at stronger vacuums.

It is noteworthy that the permeate flux becomes zero once the vacuum pressure is increased to such a value that it becomes equal to the vapor pressure of water at the feed side, that is, the driving force becomes zero.

5.1.4. Feed concentration

The influence of salt concentration on the VMD flux is shown in Fig. 8 for three different feed velocities. There is a trivial decrease in the VMD flux by increasing the feed concentration irrespective of the feed velocity. This decrease in the VMD flux is because of the reduction in the vapor pressure of water by increasing the salt concentration which is in accordance with Raoult's law [56,57]. Since the driving force for vapors transport through the membrane is the vapor pressure difference across the membrane, so by increasing
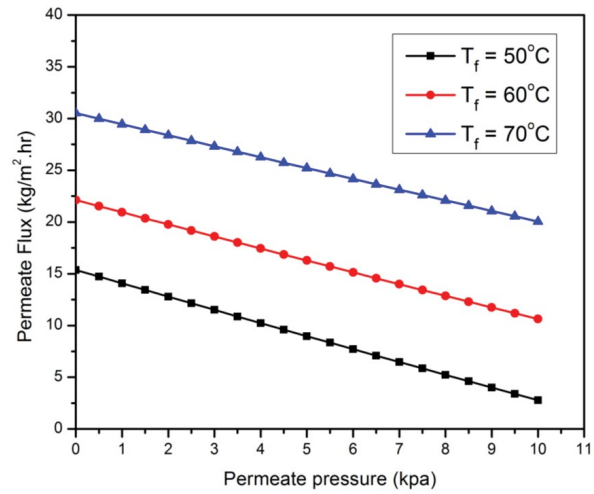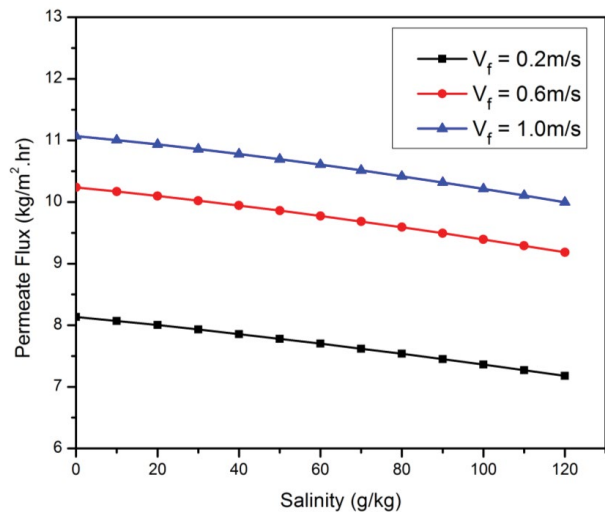

Fig. 8. Effect of salt concentration on permeate flux for feed circulation velocity (V_f) of 0.2, 0.4 and 1.0 m/s.

it at the permeate side and decreasing at the feed side, the resistance to mass transfer increases. The decrease in permeate flux with feed concentration might also be influenced by the decrease of the convective HTC with increase of solution concentration [58].

5.1.5. Heat transfer coefficient

The effect of HTC on the VMD flux is presented in Fig. 9 for three different feed temperatures (i.e., 40°C, 50°C, and 60°C). By increasing the HTC, the permeate flux increases. The increase in HTC causes the temperature difference at the feed side to decrease. Consequently, the membrane interface temperature approaches the bulk temperature and at that membrane interface temperature, the vapor pressure is higher causing an increased driving force that resulted in a greater permeate flux.
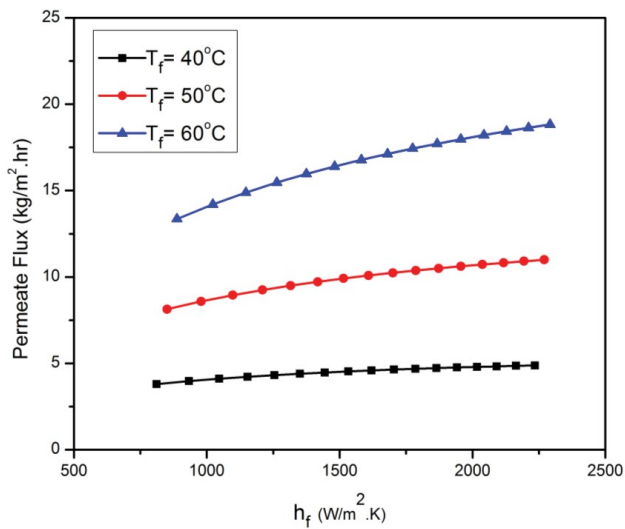
Fig. 9. Effect of heat transfer coefficient on permeate flux for three different inlet feed temperatures of 40°C, 50°C, and 60°C.

Moreover, the effect of enhancing HTC on the VMD flux is more prominent with the increase in feed temperature. In other words, increase in HTC is more effective on the VMD performance at higher feed temperatures.

5.2. Effect of operating parameters on TP

5.2.1. Feed temperature

The influence of feed temperature on TP is shown in Fig. 10a. The feed temperature was varied from 35°C to 65°C at different feed circulation velocities (i.e., 0.2, 0.4, 0.6, 0.8 and 1.0 m/s). The TPC decreases by increasing the temperature which means that the undesirable effect of TP increases with the feed temperature. This is because, rise in feed temperature increases the rate of heat transfer from feed to the permeate side and ultimately decreases the temperature at the membrane interface on the feed side. Likewise, at a higher temperature, the energy consumption from the vaporization is higher. The net result of the increased heat transfer via conduction and convection at higher feed temperature appears as a decrease in the observed TPC. Although, the TP effect increases with an increase in feed temperature, however, by increasing feed temperature, there is also an enhancement of permeate flux in all MD configurations.

5.2.2. Feed circulation velocity

Feed velocity has a significant impact on TP. As can be seen from Fig. 10b, while feed velocity is increased, the TPC increases considerably irrespective of the feed temperature and reduces the TP effect. This tendency of decreasing the TP effect can be described by the fact that an increase in the circulation velocity led to an increased HTC and minimizes boundary layer resistance. Consequently, the membrane interface temperature turns out to be closer to the bulk temperature and the TP effect diminishes.
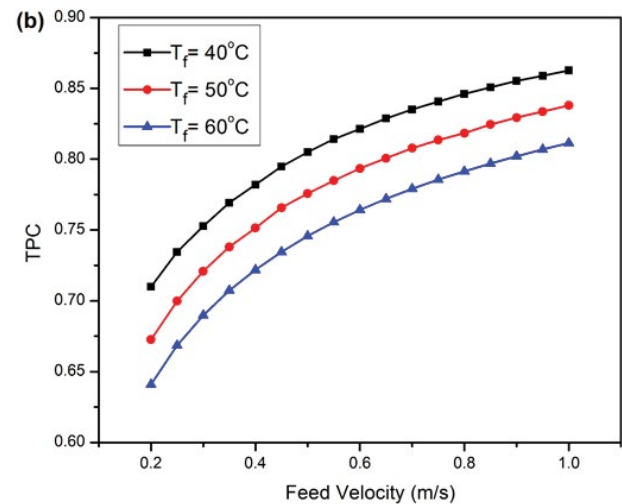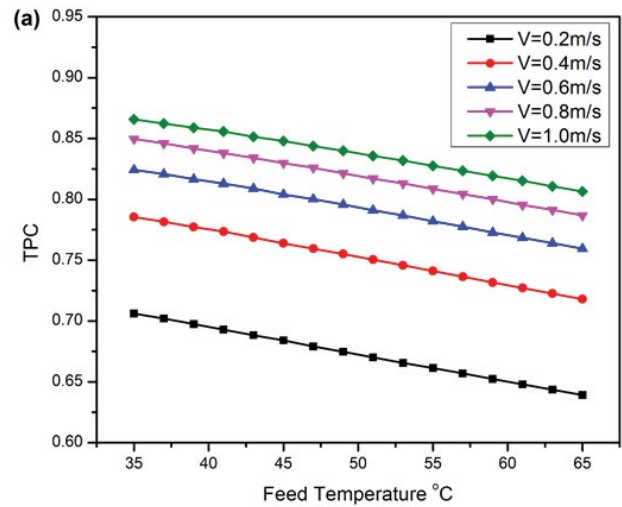

Fig. 10. Temperature polarization as a function of (a) feed temperature for five different feed circulation velocities of 0.2, 0.4, 0.6, 0.8 and 1.0 m/s and (b) feed circulation velocity for three different feed temperatures of 40°C, 50°C, and 60°C.

The increasing trend of TPC depicted that increasing the feed velocity causes an improved mixing in the feed channel which led to a reduction in the thermal boundary layer thickness. Furthermore, it is noteworthy that the change in TPC with feed velocity is more substantial at low feed velocity (laminar flow) but it becomes trivial in a turbulent flow where an increase in feed velocity does not considerably affect the TPC.

5.3. Effect of membrane characteristics on TP and permeate flux

5.3.1. Membrane porosity

Fig. 11a illustrates the influence of membrane porosity on the VMD flux. Also known as fractional void volume; membrane porosity is a major factor affecting VMD performance. Membranes having higher void volume will have a larger surface area for evaporation. As can be seen in Fig. 11a, increasing the membrane porosity results in an increased MD flux irrespective of the membrane thickness.

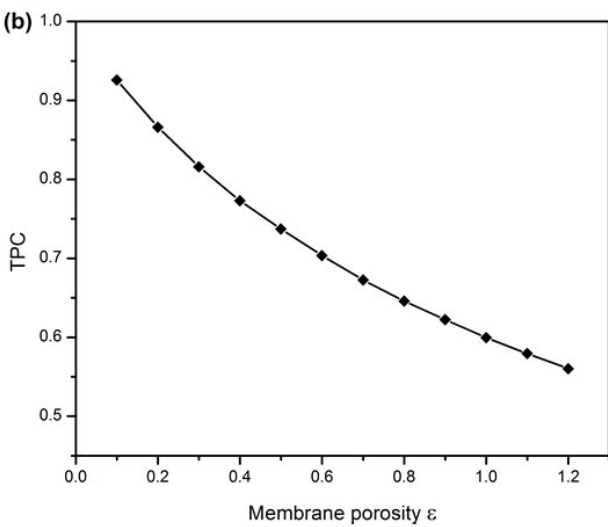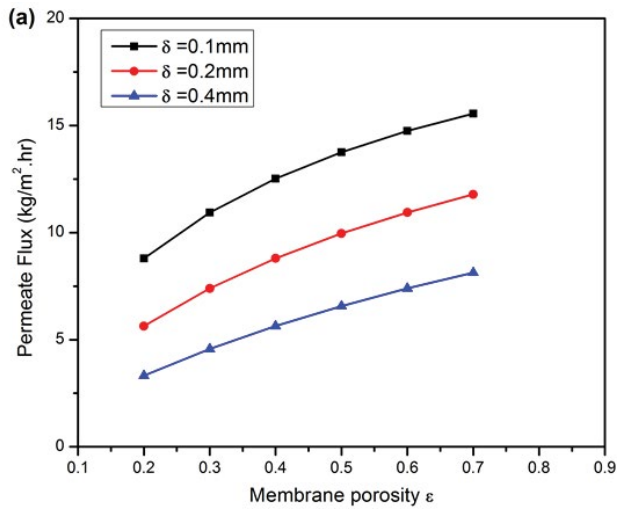Fig. 12. Effect of mean pore size (0.1–1.0 μm) on permeate flux and TP.

Fig. 11. Effect of membrane porosity on (a) permeates flux for membrane thickness (δ) of 0.1, 0.2 and 0.4 mm and (b) TP.

It must be noted that the membranes having higher porosity exhibits a lower heat loss by conduction because that the conductive HTC of the gases within the pores of the membrane is less as compared to the HTC of the hydrophobic material used in the membrane. Also, increasing the membrane porosity will result in an increased surface area of the membrane. This will cause a greater convective heat transfer and subsequently reduces the membrane interface temperature which will results in a higher TP effect as shown in Fig. 11b.

5.3.2. Mean pore size

The effect of membrane pore size on permeate flux and TP was investigated and the results are presented in Fig. 12. The feed temperature and feed circulation velocity were maintained at 50°C and 0.2 m/s, respectively. As depicted in the figure, when the mean pore size was increased from 0.1 to 1.0 μm, the permeate flux was enhanced considerably. This is because of the reduction in the mass transfer resistance with increasing pore size, which resulted in increased
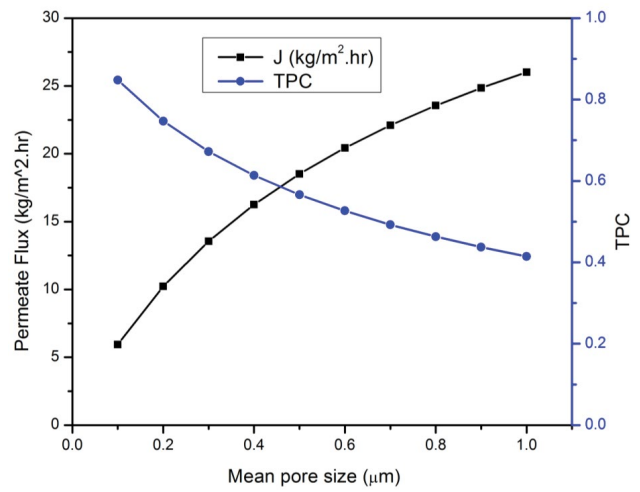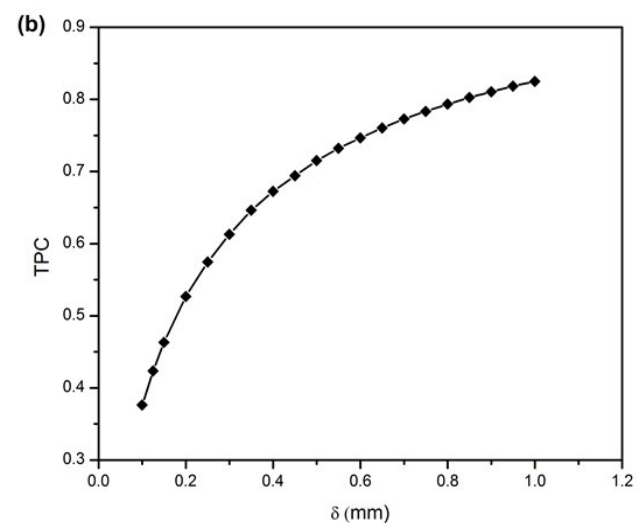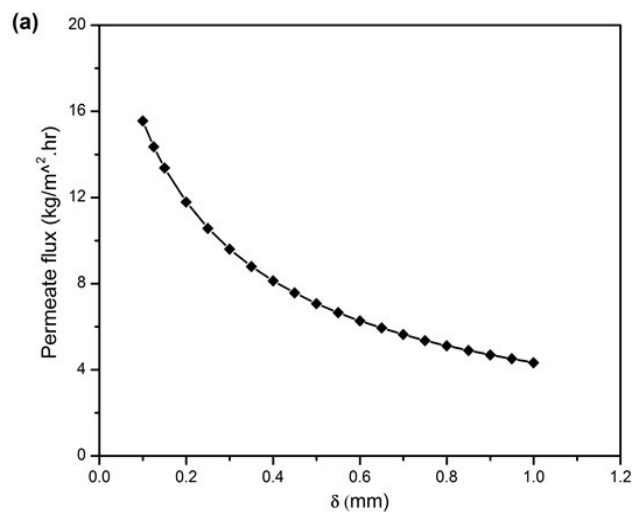

Fig. 13. Effect of membrane thickness (δ = 0.1–1.0 mm) on (a) permeate flux and (b) TP.

Table 1
Comparison of different numerical and experimentally performed VMD analysis in terms of permeate flux

Membrane material	Membrane characteristics/VMD parameters	Permeate flux	Reference
Polyvinylidene fluoride (PVDF) membrane was fabricated from Kynar® 740 using the phase inversion process	Feed temperature: 30°C; vacuum pressure: 3.78 kPa; and feed: pure water	0.71 kg/m² h	[59]
PVDF membrane was fabricated from a blend of Kynar® 740 and Kynar® HSV900 (HSV900:740 = 2:8) using phase inversion process	Feed temperature: 27.5°C and feed: 35 g/L of NaCl	0.335 kg/m² h	[60]
PVDF membrane was fabricated from a blend of Kynar® 740 and Kynar® HSV900 (HSV900:740 = 2:8) using phase inversion process	Feed temperature: 25°C; vacuum pressure: 2.306 kPa; and feed: 35 g/L of NaCl	1.25 kg/m² h	[61]
PVDF membrane was fabricated from Kynar® 740 using the immersion precipitation technique	Feed temperature: 23°C–35°C and vacuum pressure: 3.8 kPa	0.04–0.14 kg/m² h	[62]
PVDF membrane was fabricated from a blend of Kynar® 740 and Kynar® HSV900 (HSV900:740 = 4:6) using phase inversion process	Porosity: 25.32%; feed temperature: 27°C; and vacuum pressure: 3.78 kPa	0.692 kg/m² h	[63]
PVDF membrane was fabricated from Kynar® MG 15 polymer using phase inversion process	Pore size: 49.8 nm; porosity: 20.7%; feed temperature: 27°C; and vacuum pressure: 3.78 kPa	0.325 kg/m² h	[64]
PVDF membrane was prepared from Kynar® 740 using the immersion precipitation technique	Feed temperature: 30°C; vacuum pressure: 3.8 kPa; thickness: 0.25 mm	0.08 L/m² h	[65]
PP hollow fiber membrane module from Celgard Liquicel®, Hoechst-Celanese	Pore size: 0.2 μm; fiber thickness: 80 μm; Permeate pressure: 6.3–56.3 kPa; feed temperature: 25°C; feed flow rate: 1.2–2 L/min	0.3–0.5 kg/m² h	[24]
PP hollow fiber membrane	Average pore size: 0.2 μm; porosity: 60%; thickness: 0.25 mm; vacuum pressure: 4–30 kPa; feed temperature: 60°C–75°C; feed flow rate: 200–600 L/h	2.6–13.5 L/m² h	[66]
PVDF membrane were fabricated from Kynar® 740 using the phase inversion process	Feed temperature: 30°C; vacuum pressure: 3.78 kPa; and feed: 35 g/L of NaCl	0.35 kg/m² h	[59]
PP hollow fiber membrane	Pore size: 0.3 μm; feed temperature: 40°C–70°C; vacuum pressure: 10–100 mmHg; feed velocity: 0.0072–0.72 m/s; and feed: pure water	0.73–5.7 kg/m² h	[67]
PP hollow fiber membrane	Pore size: 0.3 μm; feed temperature: 40°C–70°C; vacuum pressure: 10–100 mmHg; feed velocity: 0.0072–0.72 m/s; and feed: 0.2 kg/L of NaCl	0.21–4.2 kg/m² h	[67]
PP hollow fiber membrane (MD020CP2N membrane module)	Pore size: 0.2 μm; membrane thickness: 0.4 mm; outer diameter of fibers: 2.6 mm; vacuum pressure: 4 kPa; feed temperature: 35°C–65°C; and feed velocity: 1.0 m/s	2.38–24 kg/m² h	[this work]
PP hollow fiber membrane (MD020CP2N membrane module)	Pore size: 0.2 μm; membrane thickness: 0.4 mm; outer diameter of fibers: 2.6 mm; vacuum pressure: 4 kPa; feed temperature: 60°C; and feed velocity: 0.2–1.0 m/s	13.36–19.17 kg/m² h	[this work]

vapor permeability and consequently a higher permeate flux is obtained. Also, increasing the membrane pore size resulted in an increased surface area for water evaporation which causes a decrease in the membrane interface temperature and subsequently increased the TP effect as can be seen in the figure.

5.3.3. Membrane thickness

The permeate flux decreases by increasing the membrane thickness because by increasing the thickness of the membrane, opposition to mass transfer increases as is the case in Fig. 13a. To get high VMD flux, membrane thickness should be as small as possible as depicted in the figure. On the contrary, increasing the membrane thickness would result in better heat efficiency (low TP) as shown in Fig. 13b, because in VMD the membrane itself is responsible for the conduction heat loss, and by increasing the membrane thickness the opposition to conduction heat loss increases. So, by considering both the positive effect (higher flux) and negative effect (TP) concerned with the membrane thickness, an optimum value of membrane thickness should be selected for overall VMD performance.

Table 1 shows the effects of different membrane characteristics and VMD parameters on the permeate flux studied in this work and compare to previously published data. From the table, it is clear that the VMD permeate flux depends largely upon the membrane characterization parameters as well as many process parameters such as feed circulation velocity, feed temperature, salt concentration, vacuum pressure etc.

6. Conclusion

In this paper, the VMD process is studied numerically in detail to study HMTM and also the effect of different membrane characteristics and operating parameters on the VMD performance. The results of the numerical model indicated that the VMD flux enhanced with increase of feed velocity, temperature, membrane porosity, membrane pore size, and HTC, and declined with an increase in salt concentration, vacuum pressure, and membrane thickness.

Furthermore, the following conclusions can be drawn based on this study:

- Feed concentration, feed circulation velocity, and HTC has the least impact on VMD flux as compared to vacuum pressure and feed temperature.
- The effect of feed velocity on VMD flux is trivial at low values of feed temperature; however, the effect becomes dominant with the increase in feed temperature.
- The impact of feed circulation velocity on the TP is more prominent as compared to feed temperature.
- An increase in TPC with feed velocity is more significant at low feed velocity (laminar flow) but it becomes trivial in a turbulent region where an increase in feed velocity does not considerably affect the TPC.
- Considering the effect of membrane characteristics on the VMD flux, an increase in membrane porosity and mean pore size has a positive influence on it, whereas

permeate flux decreases with an increase in membrane thickness.
- All the membrane characteristics have opposite impacts on both permeate flux and TP. Consequently, considering both the positive effect (higher permeate flux) and negative effect (TP), concerned with the membrane characteristics, an optimum value of membrane parameter should be selected for overall VMD performance.
- Increase in feed temperature results in enhanced permeate flux but on the other hand, the negative effect of TP also increases. However, feed circulation velocity has a positive impact on both the permeate flux and TP. Therefore, an increase in TP with feed temperature can be compensated by an increase in the feed velocity. Accordingly, to optimize VMD performance, high values for both the feed circulation velocity and feed temperature can be useful.

The presented results provide a comprehensive guideline for the impact of various operating conditions and membrane characteristics on permeate flux and on TP. However, it does not provide an optimum value of membrane characteristics for better performance of VMD. Therefore, for future work, it is recommended to investigate the optimum range of all membrane parameters, which will eventually improve the performance of VMD.

Abbreviations

AGMD	—	Air gap membrane distillation
DCMD	—	Direct contact membrane distillation
HTC	—	Heat transfer coefficient
HMTM	—	Heat and mass transfer model
MD	—	Membrane distillation
PP	—	Polypropylene
SGMD	—	Sweeping gas membrane distillation
TP	—	Temperature polarization
TPC	—	Temperature polarization coefficient
VMD	—	Vacuum membrane distillation
VOCs	—	Volatile organic compounds

Symbols

d_o	—	Outer diameter of fiber, mm
d_s	—	Shell inner diameter, m
h_f	—	Convection HTC at the feed side, W/m²K
J	—	Permeate flux, kg/m²h
K_f	—	Thermal conductivity of the feed solution, W/m/K
M	—	Molecular weight, kg/mol
N_f	—	Number of fibers
Nu	—	Nusselt's number
P_i	—	Partial vapor pressure of feed solution, Pa
P_v	—	Vacuum pressure, Pa
P^0	—	Vapor pressure of pure substances, Pa
Pr	—	Prandtl's number
Q_m	—	Heat transfer through the membrane
R	—	Gas constant, J/mol/K
Re	—	Reynold's number
T_b	—	Feed bulk temperature, K
T_i	—	Feed side membrane interface temperature, K
T_v	—	Temperature at the permeate side, K

Greek

δ — Membrane thickness, mm
ε — Membrane porosity
τ — Tortuosity
λ — Mean free molecular path, mm
Ø — Module packing density

Acknowledgements

References

[1] I.C. Karagiannis, P.G. Soldatos, Water desalination cost literature: review and assessment, Desalination, 223 (2008) 448–456.

[2] A.D. Khawaji, I.K. Kutubkhanah, J.-M. Wie, Advances in seawater desalination technologies, Desalination, 221 (2008) 47–69.

[3] C.-K. Chiam, R. Sarbatly, Vacuum membrane distillation processes for aqueous solution treatment—a review, Chem. Eng. Process., 74 (2013) 27–54.

[4] M. El-Bourawi, Z. Ding, R. Ma, M. Khayet, A framework for better understanding membrane distillation separation process, J. Membr. Sci., 285 (2006) 4–29.

[5] K.W. Lawson, D.R. Lloyd, Membrane distillation, J. Membr. Sci., 124 (1997) 1–25.

[6] S. Al-Obaidani, E. Curcio, F. Macedonio, G. Di Profio, H. Al-Hinai, E. Drioli, Potential of membrane distillation in seawater desalination: thermal efficiency, sensitivity study and cost estimation, J. Membr. Sci., 323 (2008) 85–98.

[7] L.-H. Cheng, Y.-H. Lin, J. Chen, Enhanced air gap membrane desalination by novel finned tubular membrane modules, J. Membr. Sci., 378 (2011) 398–406.

[8] H. Maab, L. Francis, A. Al-Saadi, C. Aubry, N. Ghaffour, G. Amy, S.P. Nunes, Synthesis and fabrication of nanostructured hydrophobic polyazole membranes for low-energy water recovery, J. Membr. Sci., 423 (2012) 11–19.

[9] M. Bahrami, J. Karimi-Sabet, A. Hatamnejad, A. Dastbaz, M.A. Moosavian, Optimization and modification of PVDF dual-layer hollow fiber membrane for direct contact membrane distillation; application of response surface methodology and morphology study, Korean J. Chem. Eng., 35 (2018) 2241–2255.

[10] B.-G. Im, J.-G. Lee, Y.-D. Kim, W.-S. Kim, Theoretical modeling and simulation of AGMD and LGMD desalination processes using a composite membrane, J. Membr. Sci., 565 (2018) 14–24.

[11] M. Safavi, T. Mohammadi, High-salinity water desalination using VMD, Chem. Eng. J., 149 (2009) 191–195.

[12] F. Laganà, G. Barbieri, E. Drioli, Direct contact membrane distillation: modelling and concentration experiments, J. Membr. Sci., 166 (2000) 1–11.

[13] M. Khayet, C. Cojocaru, Air gap membrane distillation: desalination, modeling and optimization, Desalination, 287 (2012) 138–145.

[14] M. Khayet, C. Cojocaru, A. Baroudi, Modeling and optimization of sweeping gas membrane distillation, Desalination, 287 (2012) 159–166.

[15] R.B. Saffarini, E.K. Summers, H.A. Arafat, Technical evaluation of stand-alone solar powered membrane distillation systems, Desalination, 286 (2012) 332–341.

[16] X. Chen, X. Gao, K. Fu, M. Qiu, F. Xiong, D. Ding, Z. Cui, Z. Wang, Y. Fan, E. Drioli, Tubular hydrophobic ceramic membrane with asymmetric structure for water desalination via vacuum membrane distillation process, Desalination, 443 (2018) 212–220.

[17] E. Hoffmann, D. Pfenning, E. Philippsen, P. Schwahn, M. Sieber, R. Wehn, D. Woermann, G. Wiedner, Evaporation of alcohol/water mixtures through hydrophobic porous membranes, J. Membr. Sci., 34 (1987) 199–206.

[18] N. Qureshi, M. Meagher, R. Hutkins, Recovery of 2, 3-butanediol by vacuum membrane distillation, Sep. Sci. Technol., 29 (1994) 1733–1748.

[19] Z.-P. Zhao, F.-W. Ma, W.-F. Liu, D.-Z. Liu, Concentration of ginseng extracts aqueous solution by vacuum membrane distillation. 1. Effects of operating conditions, Desalination, 234 (2008) 152–157.

[20] Z.-P. Zhao, C.-Y. Zhu, D.-Z. Liu, W.-F. Liu, Concentration of ginseng extracts aqueous solution by vacuum membrane distillation 2. Theory analysis of critical operating conditions and experimental confirmation, Desalination, 267 (2011) 147–153.

[21] R. Bagger-Jørgensen, A.S. Meyer, M. Pinelo, C. Varming, G. Jonsson, Recovery of volatile fruit juice aroma compounds by membrane technology: Sweeping gas versus vacuum membrane distillation, Innovative Food Sci. Emerg. Technol., 12 (2011) 388–397.

[22] R. Bagger-Jørgensen, A.S. Meyer, C. Varming, G. Jonsson, Recovery of volatile aroma compounds from black currant juice by vacuum membrane distillation, J. Food Eng., 64 (2004) 23–31.

[23] N. Diban, O.C. Voinea, A. Urtiaga, I. Ortiz, Vacuum membrane distillation of the main pear aroma compound: experimental study and mass transfer modeling, J. Membr. Sci., 326 (2009) 64–75.

[24] A. Hasanoğlu, F. Rebolledo, A. Plaza, A. Torres, J. Romero, Effect of the operating variables on the extraction and recovery of aroma compounds in an osmotic distillation process coupled to a vacuum membrane distillation system, J. Food Eng., 111 (2012) 632–641.

[25] Y.-R. Chen, L.-H. Chen, C.-H. Chen, C.-C. Ko, A. Huang, C.-L. Li, C.-J. Chuang, K.-L. Tung, Hydrophobic alumina hollow fiber membranes for sucrose concentration by vacuum membrane distillation, J. Membr. Sci., 555 (2018) 250–257.

[26] A. Criscuoli, E. Drioli, Vacuum membrane distillation for the treatment of coffee products, Sep. Purif. Technol., 209 (2019) 990–996.

[27] F.A. Banat, J. Simandl, Removal of benzene traces from contaminated water by vacuum membrane distillation, Chem. Eng. Sci., 51 (1996) 1257–1265.

[28] N. Couffin, C. Cabassud, V. Lahoussine-Turcaud, A new process to remove halogenated VOCs for drinking water production: vacuum membrane distillation, Desalination, 117 (1998) 233–245.

[29] Z. Jin, S.H. Zhang, X.G. Jian, Removal of 2, 4-dichlorophenol from wasterwater by vacuum membrane distillation using hydrophobic PPESK hollow hiber membrane, Chin. Chem. Lett., 18 (2007) 1543–1547.

[30] G. Sarti, C. Gostoli, S. Bandini, Extraction of organic components from aqueous streams by vacuum membrane distillation, J. Membr. Sci., 80 (1993) 21–33.

[31] J.-j. Tang, K.-g. Zhou, Q.-x. Zhang, Q.-g. Li, Study on the removal of MIBK from aqueous solution by vacuum membrane distillation, J. Cent. South Univ. T., 7 (2000) 178–181.

[32] A. Urtiaga, E. Gorri, G. Ruiz, I. Ortiz, Parallelism and differences of pervaporation and vacuum membrane distillation in the removal of VOCs from aqueous streams, Sep. Purif. Technol., 22 (2001) 327–337.

[33] A. Urtiaga, G. Ruiz, I. Ortiz, Kinetic analysis of the vacuum membrane distillation of chloroform from aqueous solutions, J. Membr. Sci., 165 (2000) 99–110.

[34] B. Wu, X. Tan, K. Li, W. Teo, Removal of 1, 1, 1-trichloroethane from water using a polyvinylidene fluoride hollow fiber membrane module: Vacuum membrane distillation operation, Sep. Purif. Technol., 52 (2006) 301–309.

[35] B. Wu, X. Tan, W. Teo, K. Li, Removal of benzene/toluene from water by vacuum membrane distillation in a PVDF hollow fiber membrane module, Sep. Sci. Technol., 40 (2005) 2679–2695.

[36] R. Baghel, S. Upadhyaya, S. Chaurasia, K. Singh, S. Kalla, Optimization of process variables by the application of response surface methodology for naphthol blue black dye removal in vacuum membrane distillation, J. Cleaner Prod., 199 (2018) 900–915.

[37] Z. Cui, Y. Zhang, X. Li, X. Wang, E. Drioli, Z. Wang, S. Zhao, Optimization of novel composite membranes for water and mineral recovery by vacuum membrane distillation, Desalination, 440 (2018) 39–47.

[38] J. Zhou, X. Zhang, B. Sun, W. Su, Performance analysis of solar vacuum membrane distillation regeneration, Appl. Therm. Eng., 144 (2018) 571–582.

[39] R. Lefers, N.S. Bettahalli, N. Fedoroff, S.P. Nunes, T. Leiknes, Vacuum membrane distillation of liquid desiccants utilizing hollow fiber membranes, Sep. Purif. Technol., 199 (2018) 57–63.

[40] S. Bandini, C. Gostoli, G. Sarti, Separation efficiency in vacuum membrane distillation, J. Membr. Sci., 73 (1992) 217–229.

[41] H. Wang, B. Li, L. Wang, S. Song, J. Wang, Y. Feng, S. Wang, Permeate flux curve characteristics analysis of cross-flow vacuum membrane distillation, Ind. Eng. Chem. Res., 51 (2011) 487–494.

[42] S.G. Lovineh, M. Asghari, B. Rajaei, Numerical simulation and theoretical study on simultaneous effects of operating parameters in vacuum membrane distillation, Desalination, 314 (2013) 59–66.

[43] J. Mengual, M. Khayet, M. Godino, Heat and mass transfer in vacuum membrane distillation, Int. J. Heat Mass Transfer, 47 (2004) 865–875.

[44] R. Schofield, A. Fane, C. Fell, Heat and mass transfer in membrane distillation, J. Membr. Sci., 33 (1987) 299–313.

[45] S. Bandini, A. Saavedra, G.C. Sarti, Vacuum membrane distillation: experiments and modeling, AIChE J., 43 (1997) 398–408.

[46] S. Shukla, J. Méricq, M. Belleville, N. Hengl, N. Benes, I. Vankelecom, J.S. Marcano, Process intensification by coupling the Joule effect with pervaporation and sweeping gas membrane distillation, J. Membr. Sci., 545 (2018) 150–157.

[47] H. Groehn, Influence of the yaw angle on heat transfer and pressure drop of helical type heat exchangers, Int. Nucl. Inf. Syst., 31 (1988).

[48] K.W. Lawson, D.R. Lloyd, Membrane distillation. I. Module design and performance evaluation using vacuum membrane distillation, J. Membr. Sci., 120 (1996) 111–121.

[49] A.S. Alsaadi, L. Francis, G.L. Amy, N. Ghaffour, Experimental and theoretical analyses of temperature polarization effect in vacuum membrane distillation, J. Membr. Sci., 471 (2014) 138–148.

[50] A.S. Alsaadi, N. Ghaffour, J.-D. Li, S. Gray, L. Francis, H. Maab, G.L. Amy, Modeling of air-gap membrane distillation process: a theoretical and experimental study, J. Membr. Sci., 445 (2013) 53–65.

[51] G. Meindersma, C. Guijt, A. De Haan, Desalination and water recycling by air gap membrane distillation, Desalination, 187 (2006) 291–301.

[52] S.P. Agashichev, A. Sivakov, Modeling and calculation of temperature-concentration polarisation in the membrane distillation process (MD), Desalination, 93 (1993) 245–258.

[53] P. Termpiyakul, R. Jiraratananon, S. Srisurichan, Heat and mass transfer characteristics of a direct contact membrane distillation process for desalination, Desalination, 177 (2005) 133–141.

[54] A.G. Fane, R. Schofield, C.J.D. Fell, The efficient use of energy in membrane distillation, Desalination, 64 (1987) 231–243.

[55] M.H. Sharqawy, J.H. Lienhard, S.M. Zubair, Thermophysical properties of seawater: a review of existing correlations and data, Desal. Wat. Treat., 16 (2010) 354–380.

[56] M. Tomaszewska, M. Gryta, A. Morawski, Study on the concentration of acids by membrane distillation, J. Membr. Sci., 102 (1995) 113–122.

[57] J.-W. Zhang, H. Fang, J.-W. Wang, L.-Y. Hao, X. Xu, C.-S. Chen, Preparation and characterization of silicon nitride hollow fiber membranes for seawater desalination, J. Membr. Sci., 450 (2014) 197–206.

[58] M. Gryta, M. Tomaszewska, Heat transport in the membrane distillation process, J. Membr. Sci., 144 (1998) 211–222.

[59] Z. Li, D. Rana, T. Matsuura, C.Q. Lan, The performance of polyvinylidene fluoride-polytetrafluoroethylene nanocomposite distillation membranes: an experimental and numerical study, Sep. Purif. Technol., 226 (2019) 192–208.

[60] Z. Li, D. Rana, Z. Wang, T. Matsuura, C.Q. Lan, Synergic effects of hydrophilic and hydrophobic nanoparticles on performance of nanocomposite distillation membranes: an experimental and numerical study, Sep. Purif. Technol., 202 (2018) 45–58.

[61] R. Zhou, D. Rana, T. Matsuura, C.Q. Lan, Effects of multi-walled carbon nanotubes (MWCNTs) and integrated MWCNTs/SiO$_2$ nano-additives on PVDF polymeric membranes for vacuum membrane distillation, Sep. Purif. Technol., 217 (2019) 154–163.

[62] Y. Yang, D. Rana, T. Matsuura, C.Q. Lan, The heat and mass transfer of vacuum membrane distillation: effect of active layer morphology with and without support material, Sep. Purif. Technol., 164 (2016) 56–62.

[63] Z. Chen, D. Rana, T. Matsuura, Y. Yang, C.Q. Lan, Study on the structure and vacuum membrane distillation performance of PVDF composite membranes: I. Influence of blending, Sep. Purif. Technol., 133 (2014) 303–312.

[64] Z. Chen, D. Rana, T. Matsuura, D. Meng, C.Q. Lan, Study on structure and vacuum membrane distillation performance of PVDF membranes: II. Influence of molecular weight, Chem. Eng. J., 276 (2015) 174–184.

[65] Y. Yang, D. Rana, T. Matsuura, S. Zheng, C.Q. Lan, Criteria for the selection of a support material to fabricate coated membranes for a life support device, RSC Adv., 4 (2014) 38711–38717.

[66] X. Wen, F. Li, X. Zhao, Filtering of low-level radioactive wastewater by means of vacuum membrane distillation, Nucl. Technol., 194 (2016) 379–386.

[67] B. Lian, Y. Wang, P. Le-Clech, V. Chen, G. Leslie, A numerical approach to module design for crossflow vacuum membrane distillation systems, J. Membr. Sci., 510 (2016) 489–496.